Hu *et al. EURASIP Journal on Advances in Signal Processing* (2016) 2016:93
DOI 10.1186/s13634-016-0388-1

EURASIP Journal on Advances in Signal Processing

RESEARCH Open Access

Ionospheric decontamination based on sparse reconstruction for skywave radar

Jinfeng Hu*, Hui Ai, Changpiao Xue, Xuan He, Wange Li, Huiyong Li, Wei Xia and Julan Xie

Abstract

Ionospheric phase decontamination is the key factor to improve the target detection capability of skywave radar. In this paper, a new ionospheric phase decontamination algorithm is proposed based on sparse reconstruction. We transform the problem of estimating ionospheric contamination phase into a sparse optimization problem, then solve it rapidly by the iterative method to get the modulation frequency caused by ionospheric phase contamination. Compared with the existing algorithms, the proposed algorithm in this paper has the following advantages: 1. higher accuracy is obtained under the situation of both fast phase fluctuation and slow phase fluctuation; 2. the proposed algorithm is more robust to noise; 3. real-data processing results of the proposed algorithm are better.

Keywords: Skywave radar, Ionospheric phase contamination, Sparse reconstruction

1 Introduction

Ionospheric instability will cause a contamination to the skywave radar echo for the radar signal propagates through the ionosphere. So, ionospheric decontamination is a very important procedure affecting target detection for skywave radar [1–3]. Ionospheric phase contamination can be regarded as a multiplicative modulation on the signal, and it will cause echo to be extended in the Doppler domain. The Doppler spectrum expansion will be worse under the situation of long coherent processing interval (CPI) [4]. The broadening of the strong sea clutter Bragg lines can smear over the nearby low-speed target spectrum. It is not conducive for the detection of low velocity target like low-speed ship. Therefore, ionospheric phase contamination compensation is one of the key factors to improve the detection capability of skywave radar [5–8].

A number of ionospheric phase decontamination methods have been proposed [9]. Bourdillon et al. [10, 11] proposed maximum entropy spectral analysis (MESA) to estimate contamination phase. But the method may fail in the case of fast phase fluctuation because fast phase fluctuation does not meet the method's assumption of linear phase in short period. Howland and Cooper [12] applied the Wigner-Ville distribution (WVD) to track the instantaneous frequency of ionospheric contamination. Unfortunately, the technique becomes invalid when there is cross term. Lu et al. [13] presented a polynomial phase signal (PPS) [14] method to compensate ionospheric phase contamination. This algorithm still works when contamination phase changes fast. But, the difficulty is that there is no effective method to choose the proper order of polynomial phase signal. To solve the above problems, Hankel rank reduction (HRR) algorithm [15] has been proposed based on constructing Hankel matrices and singular value decomposition (SVD) [16] technique. It has better performance while its accuracy still needs to be improved. To address these disadvantages, a large amount of research has been done. On the basis of HRR, You et al. [17] addressed the complex energy detection (CED) algorithm to estimate the frequency modulation component. The CED method obtains higher precision than the HRR under the situation of both slow phase fluctuation and fast phase fluctuation [18] .

In this paper, we further study the method to decontamination on the basis of CED method. Considering that the ionospheric frequency modulation function is sparse in the time-frequency domain and the sparse signal reconstruction method has the high estimation precision [19], we propose a novel phase compensation algorithm based on sparse reconstruction. Firstly, a sparse optimization problem is constructed between the ionospheric contamination phase and radar echo. Secondly, we adopt the

*Correspondence: hujf@uestc.edu.cn
Department of Electronic Engineering, University of Electronic Science and Technology of China, 611731 Chengdu, China

fast iterative method to get the ionospheric modulation frequency. At last, we compensate the raw echo by the conjugate of the contamination signal and perform fast Fourier transform (FFT) to obtain the corrected spectrum. Compared with the CED method, the algorithm proposed in this paper has the following advantages: 1. this algorithm has higher estimation precision under the situation of both slow phase fluctuation and fast phase fluctuation than the CED method; 2. this algorithm is more robust to noise. It has higher parameter estimation accuracy than the CED method in both high SNR and low SNR. Simulation results show that: 1. in the case of slow phase fluctuation, this algorithm has more than 6 dB higher estimation precision than the CED method; 2. in the case of fast phase fluctuation, the estimation precision of the proposed algorithm is more than 8 dB higher than the CED method; 3. under the situation of low SNR, this algorithm has more than 7 dB higher estimation precision than the CED method; 4. in the case of high SNR, the estimation precision of the proposed algorithm is more than 6 dB higher than the CED method. In addition, real-data processing results of the proposed algorithm are more ideal than the CED algorithm. The proposed algorithm can effectively separate the low-speed target spectrum from the Bragg peak. And, the effect on sharpening the peak spectrum is better than the CED algorithm.

This article is organized as follows. Section 2 introduces the problem analysis about ionospheric phase decontamination. Section 3 will present the proposed decontamination algorithm based on sparse reconstruction. Section 4 will give the simulation results. Section 5 will give the real data processing results. Section 6 is the conclusion of this article.

2 The analysis of ionospheric phase decontamination

The discrete form of skywave radar echo can be expressed as

$$z(k) = c(k) + w(k) + v(k), 1 \le k \le K \tag{1}$$

where z is the received radar signal, c is the sea clutter signal, w is the target signal, v is the received noise, K is the number of pulses during the CPI, and k is the slow time index.

Because of the resonant effect between the ocean surface wave and high-frequency radar signal, there are two strong Bragg peaks in the Doppler spectrum of sea clutter. The frequency of Bragg peaks is as follows

$$f_b = \pm\sqrt{\frac{gf_0}{\pi c}} \tag{2}$$

where g is the acceleration of gravity, f_0 is the carrier frequency and c is the speed of light.

Ionospheric phase contamination will cause sea clutter broadening in the Doppler domain because the sea clutter is modulated by the nonlinear phase term caused by the ionospheric movement. Therefore, we can extract the phase contamination function from the contaminated sea clutter to get the decontamination function.

Firstly, filter out the strongest Bragg peak from the radar echo by a adaptive band-pass filter. The bandwidth is suggested to be 0.5 Hz as a typical value by Howland and Cooper [12]. Taking the negative Bragg peak for example, the filtered out Bragg peak can be expressed as follows:

$$s(k) = \left[b_k^- e^{j2\pi f_b^- kT+\varphi_0} + v(k)\right] e^{j\xi(k)}, 1 \le k \le K \tag{3}$$

where $s(k)$ is the filtered out Bragg peak signal, T is the pulse repetition interval (PRI), K is the number of pulses during the CPI, k is the slow time index; b_k^-,f_b^- and φ_0 denote the amplitude, Doppler frequency and initial phase of Bragg peak, respectively; $v(k)$ denotes the white Gaussian noise; $e^{j\xi(k)}$ is the phase contamination caused by the ionospheric instability.

According to formula (3), the key of ionospheric phase decontamination is to estimate the instantaneous frequency $f(k)$ of the stretched Bragg peak. The frequency modulation function $f_r(k)$ of ionospheric contamination is formed as follows:

$$f_r(k) = f(k) - f_b \tag{4}$$

where f_b is the frequency corresponding to the filtered out Bragg peak.

By performing integration to the instantaneous ionospheric contamination frequency $f_r(k)$, the ionospheric phase contamination function $\gamma(k)$ is given as follows:

$$\gamma(k) = 2\pi \sum f_r(k) \cdot kT \tag{5}$$

where $f_r(k)$ is the frequency modulation function of ionospheric contamination, k is the slow time index and T is the pulse repetition interval.

Obviously, the more accurate the estimation of instantaneous frequency of ionospheric contamination is, the better the decontamination effect is. Better decontamination effect will be more beneficial for detecting targets. Therefore, improving the estimation precision of ionospheric frequency modulation function is the key to improving the ionospheric decontamination effect.

3 The proposed decontamination algorithm based on sparse reconstruction

The aforementioned analysis illustrates that the performance of ionospheric phase decontamination depends on the estimation accuracy of instantaneous frequency of Bragg peak.

The instantaneous frequency of Bragg peak modulated by ionospheric phase contamination is sparse in the time-frequency domain and the technique of sparse signal reconstruction has the advantage of high precision [19]. On the basis of above considerations, this paper gives a high-accuracy ionospheric phase decontamination algorithm based on sparse reconstruction.

Firstly, the estimating of instantaneous frequency of Bragg peak is converted to a sparse optimization problem through short-time inverse Fourier transform. Then, the fast iterative method is applied to solve it. The proposed algorithm simplifies the calculation of high dimension matrix in the iterative computation by fast Fourier transform (FFT) and inverse fast Fourier transform (IFFT), which will greatly reduce the amount of computation. Compared with the existing algorithms, the proposed algorithm in this paper obtains high precision under the situation of both slow and fast phase fluctuation and better robustness to noise.

3.1 The sparse representation of contamination phase

The filtered out Bragg peak in formula (3) can be formed by orthogonal basis of the short time Fourier transform (STFT) as follows [8]

$$s(k) = \frac{1}{N}\sum_{n=1}^{K}\sum_{m=1}^{K} S(m,n)g(k-n)e^{j\frac{2\pi}{N}mk}, 1 \le k \le K \tag{6}$$

where $g(k)$ is the window function, and in this paper the hamming window is adopted for its low sidelobe, $s(k)$ is the kth element of the filtered out Bragg peak in formula (3), $S(m,n)$ is the mth row nth column element of the STFT time-frequency distribution matrix of Bragg peak, where m and n represent the time dimension and frequency dimension, respectively. Formula (6) can be abbreviated as follows

$$\mathbf{s} = \frac{1}{\sqrt{N}}\mathbf{ATx} \tag{7}$$

where s is the signal column vector of the filtered out Bragg peak with the length of K, $\mathbf{x}$ is the rearranged time-frequency distribution matrix $S(m,n)$ in column and the rearrangement is $\mathbf{x}[\,kK-K+1 : kK, 1] = S[:,k]\,, k = 1, 2, \cdots, K$. $\mathbf{x}$ is the instantaneous frequency of Bragg peak modulated by ionospheric phase contamination, which is sparse in the time-frequency domain. $\mathbf{A} \in \mathbb{R}^{K\times K^2}$ is a sparse row block matrix composed of K diagonal matrixes as formula (8). The diagonal elements of $\mathbf{A}_i$ are the sliding window function $g(k-i)$ as formula (9).

$$\mathbf{A} = \left[\begin{array}{cccc}\mathbf{A}_1 & \mathbf{A}_2 & \cdots & \mathbf{A}_K\end{array}\right] \tag{8}$$

$$\mathbf{A}_i = \left[\begin{array}{cccc} g(1-i) & 0 & \cdots & 0 \\ 0 & g(2-i) & \cdots & 0 \\ \vdots & \vdots & \ddots & \vdots \\ 0 & 0 & \cdots & g(K-i)\end{array}\right] \tag{9}$$

$\mathbf{T} \in \mathbb{C}^{K^2\times K^2}$ is a block diagonal matrix with K diagonal blocks, as formula (10). Each diagonal block matrix $\mathbf{T}_i$ has the same size of $K \times K$, the element in $\mathbf{T}_i$ is $\mathbf{T}_i(m,n) = 1/\sqrt{K}\cdot e^{j\frac{2\pi}{K}mn}, m, n = 1, 2, \cdots, K$.

$$\mathbf{T} = \left[\begin{array}{cccc}\mathbf{T}_1 & 0 & \cdots & 0 \\ 0 & \mathbf{T}_2 & \cdots & 0 \\ \vdots & \vdots & \ddots & \vdots \\ 0 & 0 & \cdots & \mathbf{T}_K\end{array}\right] \tag{10}$$

It is obvious that $\mathbf{T}_i$ is the inverse Fourier transform matrix. Because of ${\mathbf{T}_i}^{-1} = {\mathbf{T}_i}^H$, the inverse matrix ${\mathbf{T}_i}^{-1}$ of $\mathbf{T}_i$ is the Fourier transform matrix. According to the property of $\mathbf{T}_i$ and ${\mathbf{T}_i}^{-1}$, the product $\mathbf{T}_i\mathbf{a}$ and ${\mathbf{T}_i}^{-1}\mathbf{a}$ is equal to the inverse fast Fourier transform (IFFT) and the fast Fourier transform (FFT) of $\mathbf{a}$ which is a column vector with K elements. The mathematical expressions are shown as follows:

$$\mathbf{T}_i\mathbf{a} = \sqrt{K}\mathrm{IFFT}(\mathbf{a}) \tag{11}$$

$${\mathbf{T}_i}^{-1}\mathbf{a} = \frac{1}{\sqrt{K}}\mathrm{FFT}(\mathbf{a}) \tag{12}$$

For simplification, let $\mathbf{y} = \sqrt{N}\mathbf{s}$, formula (7) can be expressed as:

$$\mathbf{y} = \mathbf{ATx} \tag{13}$$

Formula (13) is a sparse optimization problem because $\mathbf{x}$ is sparse in the time-frequency domain.

3.2 The sparse iterative algorithm of ionospheric phase decontamination

In order to solve Eq. (13), we transform the equation to a convex optimization problem as follows

$$\mathbf{x} = \arg\min_{\mathbf{x}} \|\mathbf{x}\|_1 \quad \text{s.}t. \quad \left\|\mathbf{ATx}-\mathbf{y}\right\|_2^2 \le \beta \tag{14}$$

where $\|\mathbf{x}\|_1 = \sum_{i=1}^{i=K^2}|x(i)|$ is the ℓ_1 norm of vector $\mathbf{x}$.

In formula (14), the minimum ℓ_1 norm has the problem of oversparse. In order to circumvent the problem, we constrain the energy distribution of $\mathbf{x}$ in this paper. Through the minimum ℓ_2 norm, the energy of $\mathbf{x}$ will be dispersed to every dimension. So, we add ℓ_2 norm of $\mathbf{x}$ to formula (14). The mixed $\ell_1 - \ell_2$ norm is adopted in this paper as formula (15), where $\|\mathbf{x}\|_2^2 = \sum_{i=1}^{i=K^2}|x(i)|^2$ is the square of $\mathbf{x}$'s ℓ_2 norm and α is the weighted coefficient of ℓ_2 norm.

$$\mathbf{x} = \arg\min_{\mathbf{x}}\left(\|\mathbf{x}\|_1 + \frac{\alpha}{2}\|\mathbf{x}\|_2^2\right) \ \text{s.}t. \ \left\|\mathbf{ATx}-\mathbf{y}\right\|_2^2 \le \beta \tag{15}$$

A fast iterative algorithm is adopted to solve formula (15). The iterative procedure is given as follows:

$$\mathbf{x}_{k+1} = \arg\min_{\mathbf{x}} \left(\|\mathbf{x}\|_1 + \frac{\alpha}{2} \|\mathbf{x}\|_2^2 + \frac{\lambda}{2} \left\|\mathbf{A}\mathbf{T}\mathbf{x} - \mathbf{y}_k\right\|_2^2 \right) \tag{16}$$

$$\mathbf{y}_{k+1} = \mathbf{y} + \mathbf{y}_k - \mathbf{A}\mathbf{T}\mathbf{x}_{k+1} \tag{17}$$

Through the iterative calculation of Eqs. (16) and (17), we can get the value of $\mathbf{x}_k$. Then, calculate the error $\left\|\mathbf{A}\mathbf{T}\mathbf{x}_{\mathrm{k}} - \mathbf{y}\right\|_2^2$ and stop the iteration if the error is smaller than the set β.

To solve Eq. (16) simply, a new vector $\mathbf{c}$ is used to approach $\mathbf{x}$ to separate the ℓ_1 and ℓ_2 norm of $\mathbf{x}$ by substituting $\mathbf{c}$'s ℓ_1 norm for $\mathbf{x}$'s ℓ_1 norm. Then, Eq. (16) is transformed into Eqs. (18) and (19).

$$\begin{aligned}\left(\mathbf{x}_{k+1}, \mathbf{c}_{k+1}\right) = \arg\min_{\mathbf{x},\mathbf{c}} \Big(&\|\mathbf{c}\|_1 + \frac{\alpha}{2} \|\mathbf{x}\|_2^2 \\ &+ \frac{\lambda}{2} \left\|\mathbf{A}\mathbf{T}\mathbf{x} - \mathbf{y}_k\right\|_2^2 \\ &+ \frac{\gamma}{2} \|\mathbf{c} - \mathbf{x} - \mathbf{b}_k\|_2^2 \Big)\end{aligned} \tag{18}$$

$$\mathbf{b}_{k+1} = \mathbf{b}_k + \mathbf{x}_{k+1} - \mathbf{c}_{k+1} \tag{19}$$

It is easy to figure out $\mathbf{x}_{k+1}$ and $\mathbf{c}_{k+1}$, respectively in Eq. (18) as formula (20) and (21).

$$\begin{aligned}\mathbf{x}_{k+1} = \arg\min_{\mathbf{x}} \Big(&\frac{\alpha}{2} \|\mathbf{x}\|_2^2 + \frac{\lambda}{2} \left\|\mathbf{A}\mathbf{T}\mathbf{x} - \mathbf{y}_k\right\|_2^2 \\ &+ \frac{\gamma}{2} \|\mathbf{c}_k - \mathbf{x} - \mathbf{b}_k\|_2^2 \Big)\end{aligned} \tag{20}$$

$$\mathbf{c}_{k+1} = \arg\min_{\mathbf{c}} \left(\|\mathbf{c}\|_1 + \frac{\gamma}{2} \left\|\mathbf{c} - \mathbf{x}_{k+1} - \mathbf{b}_k\right\|_2^2 \right) \tag{21}$$

In Eq. (20), α denotes the weighting factor of ℓ_2 norm. The value will affect the aggregation of the obtained time-frequency spectrum. If $\alpha \to 0$, the result will be oversparse, and if $\alpha \to \infty$, the solution converges to the nonsparse result with the minimum ℓ_2 norm. Equation (20) can be solved by the simple differential operation. To simplify the calculation in formula (20), let $\mathbf{d} = \mathbf{T}\mathbf{x}$ and solve $\mathbf{d}$ firstly as formula (22). Then, obtain $\mathbf{x}$ by $\mathbf{x} = \mathbf{T}^H\mathbf{d}$. It is easy to solve Eq. (21) by the shrink operation as formula (23).

$$\mathbf{d}_{k+1} = \left[(\alpha + \gamma)\mathbf{I} + \lambda\mathbf{A}^H\mathbf{A}\right]^{-1} \left[\lambda\mathbf{A}^H\mathbf{y}_k + \gamma\mathbf{T}\left(\mathbf{c}_k - \mathbf{b}_k\right)\right] \tag{22}$$

$$\mathbf{c}_{k+1} = \mathrm{shrink}\left(\mathbf{x}_{k+1} + \mathbf{b}_k, \frac{1}{\gamma}\right) \tag{23}$$

The shrink operator in formula (23) is given as follows:

$$\mathrm{shrink}(\mathbf{w}, a) = \frac{\mathbf{w}}{|\mathbf{w}|} \max(|\mathbf{w}| - a, 0)\} \tag{24}$$

By rearranging the column vector x into a matrix with the size of $K \times K$, we obtain the sparse time-frequency distribution matrix of the filtered out Bragg peak s. At each time snapshot, we select the peak, then obtain the instantaneous frequency $f(k)$ of the Bragg peak. According to $f(k)$ and formula (4), ionospheric phase contamination function $\gamma(k)$ can be obtained by formula (5). The contamination correction function is the conjugate of phase contamination function. Then, perform the decontamination to the echo data as follows:

$$z_1(k) = z(k) \cdot e^{-j\gamma(k)}, 1 \le k \le K \tag{25}$$

where $e^{-j\gamma(k)}$ is the ionospheric phase decontamination function, $z(k)$ is the received radar signal in formula (1), and $z_1(k)$ is the signal after decontamination.

The proposed ionospheric decontamination algorithm in this paper is summarized as follows:

1. Transform the received signal $z(k)$ into frequency domain via FFT.
2. Filter out the strongest Bragg peak in the frequency domain.
3. Perform IFFT and get the Bragg peak signal $\mathbf{s}$.
4. Compute the instantaneous frequency of $\mathbf{s}$ according to the following steps:
   Initialize: $\mathbf{y} = \sqrt{N}\mathbf{s}, \mathbf{A}, \mathbf{T}, \alpha, \lambda, \gamma, \beta, \mathbf{d}_0 = \mathbf{A}^T\mathbf{y}, \mathbf{W} = (\alpha + \gamma)\mathbf{I} + \lambda\mathbf{A}^H\mathbf{A}, \mathbf{y}_k = \mathbf{y}, \mathbf{b}_0 = \mathbf{0}, \mathbf{c}_0 = \mathbf{0}$
   While $\left\|\mathbf{A}\mathbf{d}_k - \mathbf{y}\right\|_2^2 > \beta$
   $\mathbf{d}_{k+1} = \mathbf{W}^{-1}\left[\lambda\mathbf{A}^H\mathbf{y}_k + \gamma\mathbf{T}(\mathbf{c}_k - \mathbf{b}_k)\right]$
   $\mathbf{c}_{k+1} = \mathrm{shrink}\left(\mathbf{T}^{-1}\mathbf{d}_{k+1} + \mathbf{b}_k, \frac{1}{\gamma}\right)$
   $\mathbf{b}_{k+1} = \mathbf{b}_k + \mathbf{T}^{-1}\mathbf{d}_{k+1} - \mathbf{c}_{k+1}$
   $\mathbf{y}_{k+1} = \mathbf{y} + \mathbf{y}_k - \mathbf{A}\mathbf{d}_{k+1}$
   End
   $\mathbf{x} = \mathbf{T}^H\mathbf{d}_k$
5. Rearrange the vector x and obtain the sparse time-frequency distribution matrix of the filtered out Bragg peak s.
6. Search the peak of the sparse time-frequency distribution matrix at each time snapshot, and obtain the instantaneous frequency $f(k)$ of the Bragg peak.
7. Compute the frequency modulation function of ionospheric contamination $f_r(k) = f(k) - f_b$.
8. Compute the ionospheric phase contamination function $\gamma(k) = 2\pi \sum f_r(k) \cdot kT$.
9. Perform the decontamination to the received signal $z(k)$ by $z_1(k) = z(k) \cdot e^{-j\gamma(k)}, 1 \le k \le K$.

In the proposed algorithm, we use FFT and IFFT to simplify the multiplications of large-scale block diagonal matrix $\mathbf{T}$ and $\mathbf{T}^{-1}$. The calculation of $\mathbf{T}(\mathbf{c}_k - \mathbf{b}_k)$

and $\mathbf{T}^{-1}\mathbf{d}_{k+1}$ is given as follows: firstly, divide the vector $\mathbf{c}_k - \mathbf{b}_k$ and $\mathbf{d}_{k+1}$ into K segments and each segment contains K elements. Secondly, perform IFFT or FFT to each segment data. Therefore, the multiplications $\mathbf{T}(\mathbf{c}_k - \mathbf{b}_k)$ and $\mathbf{T}^{-1}\mathbf{d}_{k+1}$ only need performing IFFT or FFT K times. It greatly reduces the amount of calculation. The computation is $O(N^2\log_2 N)$. The mathematical expressions are given in formula (26) and (27). $\mathrm{IFFT}_K(\mathbf{c}_k - \mathbf{b}_k)$ and $\mathrm{FFT}_K(\mathbf{d}_{k+1})$ denote that divide the vector $\mathbf{c}_k - \mathbf{b}_k$ and $\mathbf{d}_{k+1}$ into K segments, then perform IFFT and FFT for each segment and arrange the results of K segments into a column vector.

$$\mathbf{T}(\mathbf{c}_k - \mathbf{b}_k) = \sqrt{K}\mathrm{IFFT}_K(\mathbf{c}_k - \mathbf{b}_k) \tag{26}$$

$$\mathbf{T}^{-1}\mathbf{d}_{k+1} = \frac{1}{\sqrt{K}}\mathrm{FFT}_K(\mathbf{d}_{k+1}) \tag{27}$$

In the algorithm, $\mathbf{A}$ is a row block diagonal matrix, so the nonzero elements of $\mathbf{W} = (\alpha + \gamma)\mathbf{I} + \lambda\mathbf{A}^H\mathbf{A}$ only distribute in the $2n - 1$ lines around the diagonal line, where n is the length of the window function. Both $\mathbf{W}$ and $\mathbf{W}^{-1}$ have at most $K(n^2 - n + K)$ nonzero elements, so it is easy to obtain accurate $\mathbf{W}^{-1}$. $\mathbf{W}^{-1}$ is stored prior to iterating, so the calculation won't increase. In addition, the computation of shrink operator is very small. So, in the proposed algorithm, the amount of calculation in each iteration is mainly caused by calculating $\mathbf{T}(\mathbf{c}_k - \mathbf{b}_k)$ and $\mathbf{T}^{-1}\mathbf{d}_{k+1}$ whose calculation have been reduced to $O(N^2\log_2 N)$ through FFT and IFFT. Therefore, the proposed algorithm in this paper satisfies fast solution in engineering.

4 Simulation results

The simulation results in Sections 4.1 and 4.2 show that the proposed algorithm has higher estimation accuracy and better decontamination effect than CED algorithm in the case of both slow and fast phase fluctuation. According to the simulation results in Section 4.3, in both low SNR and high SNR, the proposed algorithm still has higher estimation accuracy than CED algorithm.

Table 1 is the simulation parameters used in Sections 4.1 and 4.2. In this paper, α, β, γ is 0.4, 0.2 and 0.4, respectively. This article adopts the ionospheric phase contamination function $\gamma(t) = M\cos\left(2\pi f_m t + \theta_0\right)$ [15], which is adopted in a large body of literature. M and f_m denote the amplitude and frequency of the phase contamination function. The corresponding ionospheric frequency modulation function of the phase contamination is $f_r(t) = -Mf_m \sin\left(2\pi f_m t + \theta_0\right)$. Mf_m is the amplitude of modulation frequency. f_m denotes the frequency of phase fluctuation. Big and small f_m correspond to fast and slow phase fluctuation, respectively. Simulation results show that the proposed algorithm is more accurate than CED algorithm and has a better decontamination effect. Besides, the simulation results at different SNR (20 – 50 dB) show that the estimation accuracy of the proposed algorithm is higher than that of CED algorithm in both low SNR and high SNR.

Table 1 Simulation parameters

f_0	15 MHz	K	512
g	9.8 m/s2	T	0.1 s
CNR	30 dB	SNR	5 dB
	Doppler frequency of Bragg f_b		±0.3949 Hz
	Amplitude of negative Bragg b_k^-		7
	Amplitude of positive Bragg b_k^+		5
	Doppler frequency of target f_t		0.6 Hz

4.1 Simulations under slow phase fluctuation

The following simulation results show that, under slow phase fluctuation, the estimation accuracy of the proposed algorithm is higher than that of CED algorithm and the decontamination effect is better than CED algorithm.

In the condition of f_m=0.05 Hz and $Mf_m = 0.1$, the phase fluctuation is slow. Figure 1 displays the estimated instantaneous frequency of the filtered out Bragg peak by the proposed algorithm and CED algorithm compared with the theory frequency. Regardless of the fixed Bragg frequency, we only focus on the variation of the modulated frequency caused by ionospheric contamination in Fig. 1. Figure 1 shows that the estimated instantaneous frequency by the proposed algorithm is closer to the theory frequency, so the estimation accuracy of the proposed algorithm is higher than the CED algorithm.

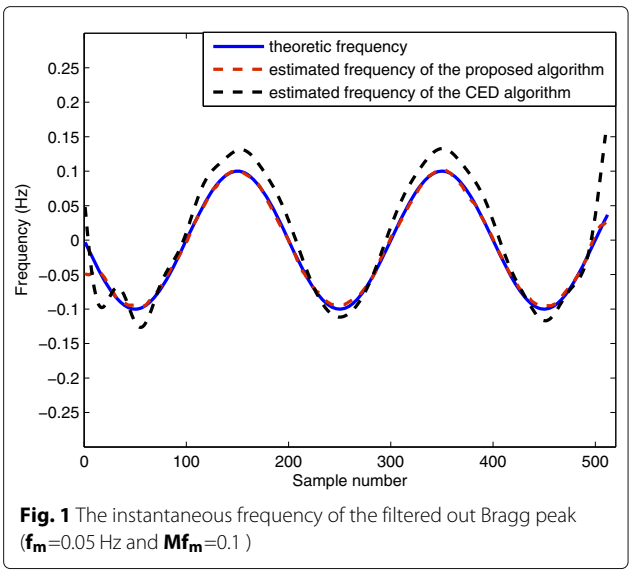

Fig. 1 The instantaneous frequency of the filtered out Bragg peak ($\mathbf{f_m}$=0.05 Hz and $\mathbf{Mf_m}$=0.1)

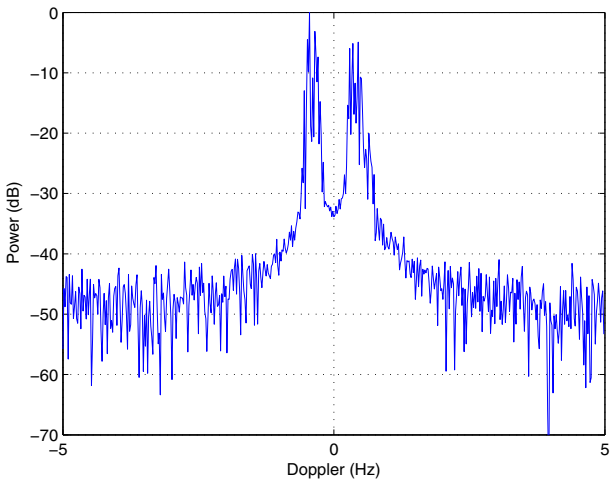

Fig. 2 The Doppler spectrum of the contaminated signal ($\mathbf{f_m}$=0.05 Hz and $\mathbf{Mf_m}$=0.1)

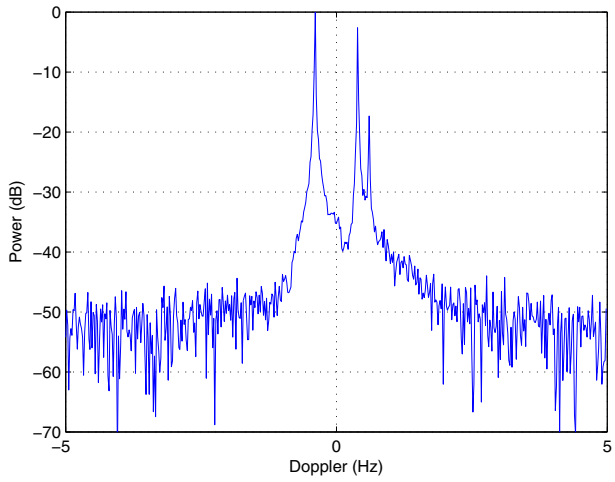

Fig. 4 The decontaminated signal spectrum by the proposed algorithm ($\mathbf{f_m}$=0.05 Hz and $\mathbf{Mf_m}$=0.1)

Next, we use the estimated modulation frequency by the proposed algorithm and CED algorithm (in Fig. 1) to compensate the contaminated signal, respectively. Figure 2 is the Doppler spectrum of the contaminated signal without decontamination. The expansion of sea clutter spectrum and the target spectrum is serious. The strong broadening Bragg peaks spectrum will mask the target spectrum, which makes it difficult to detect targets. Figure 3 is the decontaminated signal spectrum by the CED algorithm. There are many glitches around the Bragg peaks caused by the residual phase contamination because of the inaccurate estimation of the contamination frequency. The target spectrum is buried in these glitches. Figure 4 is the signal spectrum compensated by the proposed algorithm. The spectrum after decontamination becomes very sharp. The Doppler spectrum of the target can be discriminated clearly. Comparing these simulation results, the proposed algorithm's decontamination performance is better than the effect of CED algorithm under slow phase fluctuation.

4.2 Simulations under fast phase fluctuation

The following simulations show that, in the case of fast phase fluctuation, the proposed algorithm has higher estimation precision and better performance of decontamination than the CED algorithm.

Under the situation of fast phase fluctuation (f_m = 0.25 Hz and Mf_m=0.1), Fig. 5 displays the instantaneous frequency of the filtered out Bragg peak estimated by the proposed algorithm and CED algorithm compared with

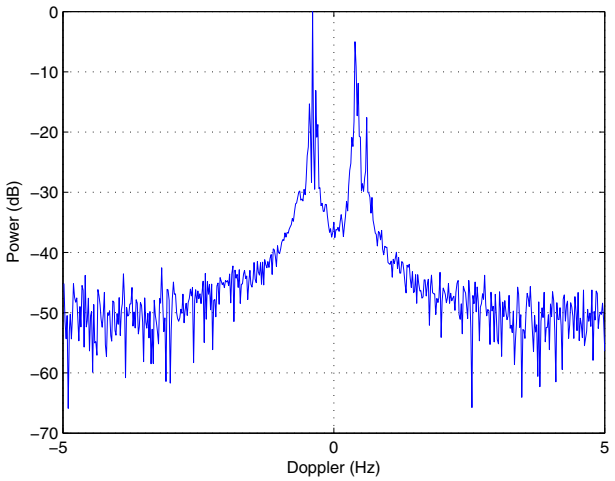

Fig. 3 The decontaminated signal spectrum by the CED algorithm ($\mathbf{f_m}$=0.05 Hz and $\mathbf{Mf_m}$=0.1)

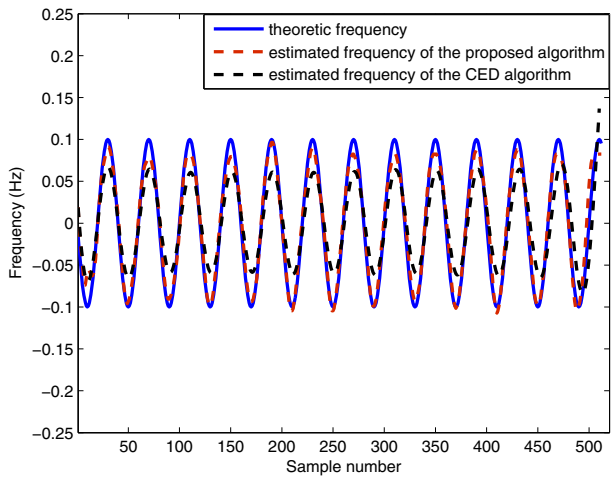

Fig. 5 The estimated instantaneous frequency of the filtered out Bragg peak ($\mathbf{f_m}$ = 0.25 Hz and $\mathbf{Mf_m}$ = 0.1)

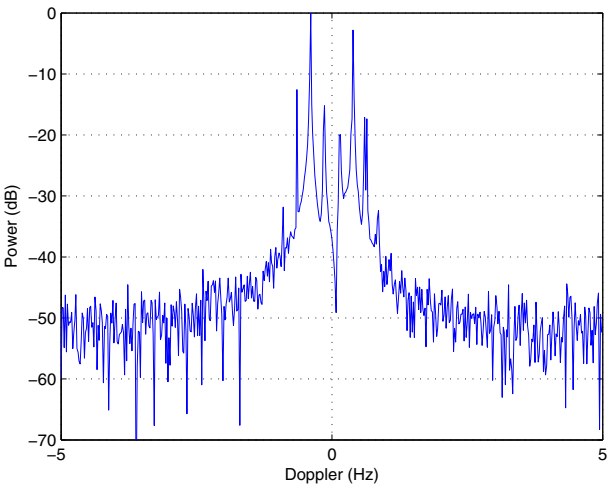

Fig. 6 The Doppler spectrum of the contaminated signal ($\mathbf{f_m}$=0.25 Hz and $\mathbf{Mf_m}$=0.1)

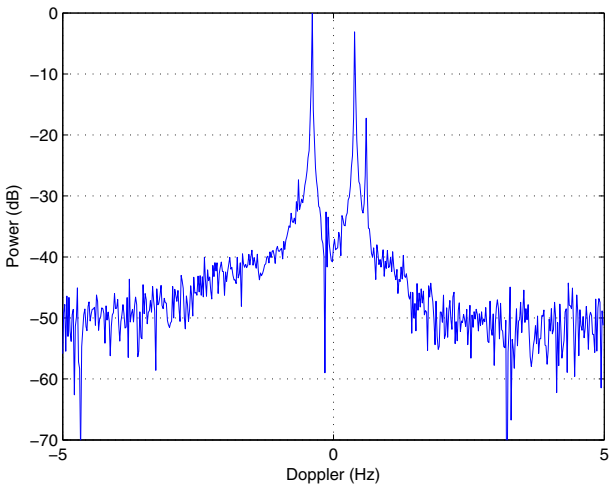

Fig. 8 The decontaminated signal spectrum by the proposed algorithm ($\mathbf{f_m}$=0.25 Hz and $\mathbf{Mf_m}$=0.1)

the theory frequency. The variation of the modulated frequency caused by ionospheric contamination is shown in Fig. 5. Compared with CED algorithm, the estimated contamination frequency of the proposed algorithm is closer to the actual frequency, so the estimation precision of the proposed algorithm is higher.

Then, we use the ionospheric contamination frequency estimated by the proposed algorithm and CED algorithm (in Fig. 5) to decontaminate the signal, respectively. Figure 6 is the Doppler spectrum of the original signal without decontamination. The sea clutter spectrum and the target spectrum is broadening. The expansion of strong Bragg peaks makes detecting targets difficult. Figure 7 is the signal spectrum corrected by the CED algorithm. The residual phase contamination generates the glitches around the Bragg peaks for the inaccurate estimation of the contamination frequency. It is bad for detecting targets because the target spectrum is buried in these glitches. Figure 8 is the signal spectrum corrected by the proposed algorithm. The spectrum of the corrected signal is very sharp. The Doppler spectrum of Bragg peaks and the target is separated clearly. Comparing Figs. 7 and 8, the proposed algorithm has better decontamination performance than the CED algorithm under fast phase fluctuation.

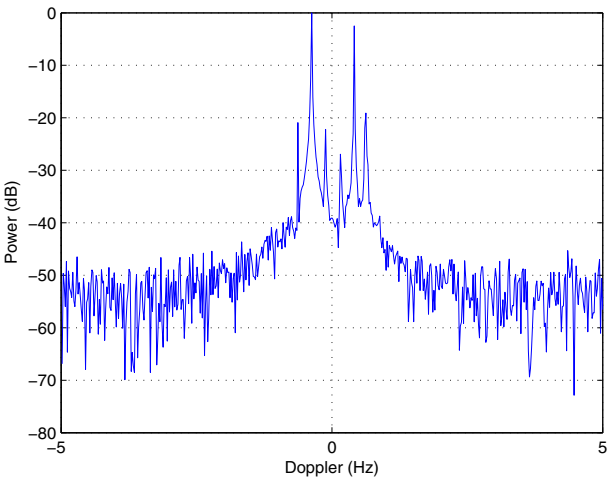

Fig. 7 The decontaminated signal spectrum by the CED algorithm ($\mathbf{f_m}$=0.25 Hz and $\mathbf{Mf_m}$=0.1)

4.3 Simulations in different SNR

Figure 9 shows the estimation frequency's mean square error (MSE) in different SNR of the proposed algorithm and CED algorithm. The MSE is defined as $mse = \frac{1}{N}\sum_{n=1}^{N}\left|f(\mathrm{n}) - \widehat{f}(n)\right|^2$. A complex frequency modulated signal is adopted in the simulation. The parameters are as follows: the center frequency is 0.5 Hz, the phase fluctuation frequency varies from 0.05 to 0.25 Hz with a interval of 0.05 Hz, the sampling frequency is 10 Hz, the sampling point is 512 and the SNR varies from 20 to 50 dB. Figure 9 illustrates that if the phase fluctuation frequency f_m is a fixed value, the higher the SNR is, the smaller the MSE is, and the higher the estimation precision is; if the SNR is fixed, the smaller the phase fluctuation frequency f_m is, the smaller the mean square error is, and the higher the estimation precision is.

Comparing the MSE lines of the proposed algorithm and the CED algorithm in Fig. 9, we can get that: in the case of slow phase fluctuation (f_m=0.05 Hz), the accuracy of the proposed algorithm is 7 dB (SNR=20 dB) and 6 dB (SNR=50 dB)

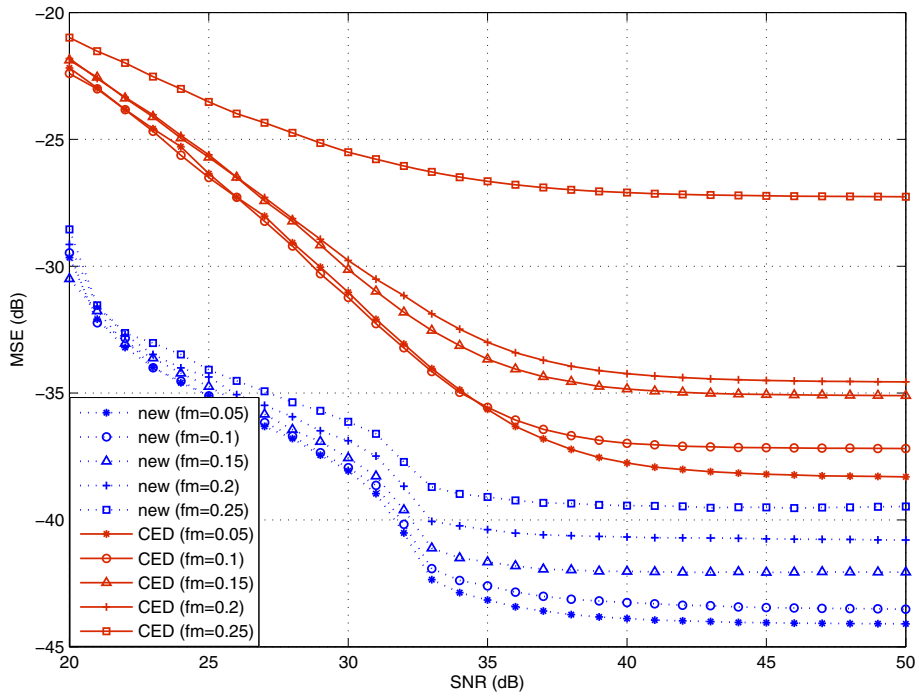

Fig. 9 MSE of the proposed algorithm and the CED algorithm (SNR=20–50 dB)

higher than the CED algorithm, respectively; furthermore, under the situation of fast phase fluctuation (f_m=0.25 Hz), the accuracy of the proposed algorithm is 8 dB (SNR=20 dB) and 12 dB (SNR=50 dB) higher than the CED algorithm, respectively. Therefore, the proposed algorithm has a higher estimation accuracy than the CED algorithm no matter in the case of both high and low SNR or under the situation of both fast and slow phase fluctuation.

5 Real-data processing results

In this section, the Skywave radar real data is processed to prove the proposed algorithm and compared with the CED algorithm. The data comes from a practical skywave radar. For the first echo, the working frequency is 21.39 MHz, the bandwidth is 0.16 MHz, the pulse repetition period is 0.1S, and the pulse accumulation number is 512. For the second echo, the working frequency is 14.76 MHz, the bandwidth is 0.01 MHz, the pulse repetition period is 0.012S, and the pulse accumulation number is 512.

Figure 10 is the Doppler spectrum of a distance cell of the first echo. The positive Bragg peak is located at about 0.5 Hz, and the negative Bragg peak is located at about −0.45 Hz. Two low speed ship targets are located at 0 and 1.1 Hz, respectively. Due to the ionospheric phase contamination, the Doppler broadening exists in the sea clutter spectrum and the target spectrum. The target spectrum at 1.1 Hz and the positive Bragg peak are mixed thus they are hard to be detected.

Figure 11 is the result of the proposed algorithm. From Fig. 11, it is obvious that the sea clutter spectrum and the target spectrum are obviously sharpened after the decontamination of the proposed algorithm. The target spectrum at 0 Hz is higher and more clear. And, the target spectrum at 1.1 Hz is separated from the positive Bragg peak effectively, which can be easily detected.

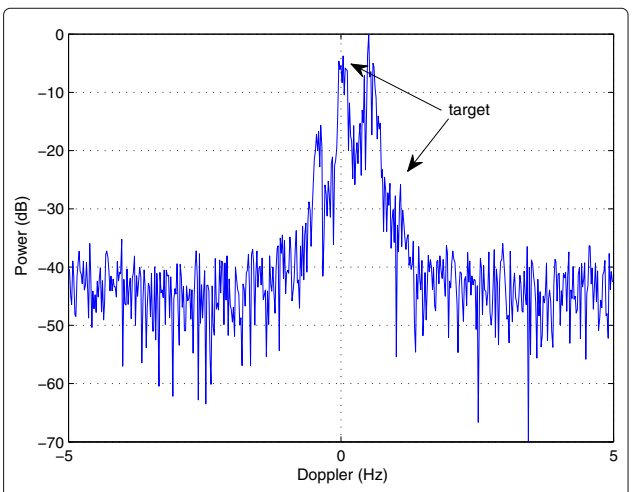

Fig. 10 The Doppler spectrum of the real signal

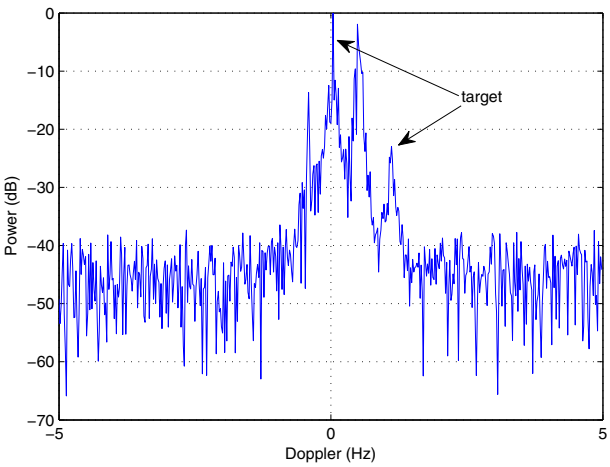

Fig. 11 The decontaminated real signal spectrum by the proposed algorithm

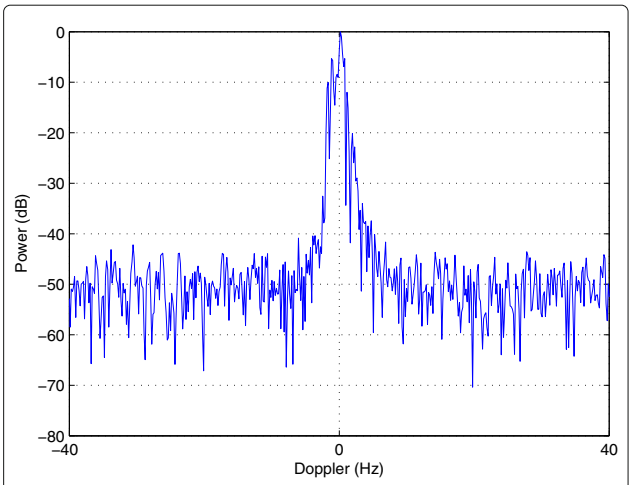

Fig. 13 The Doppler spectrum of the real signal

Figure 12 is the result of the CED algorithm. In Fig. 12, the noise floor is slightly higher, the negative Bragg peak and the target spectrum at 0 Hz are relatively sharpened, but the effect is less ideal than the proposed algorithm. Besides, the CED algorithm can not visibly distinguish the target at 1.1 Hz from the positive Bragg peak.

Figure 13 is the Doppler spectrum of a distance cell of the second echo. Because of the low doppler resolution and the large phase perturbation, the sea clutter is seriously broadened, and the Bragg peaks overlap at about 0 Hz.

Figure 14 is the result of the proposed algorithm. Figure 15 is the result of the CED algorithm. From the figures, the sea clutter is obviously narrowed by the proposed algorithm but the effect of the CED algorithm is almost invisible.

The above two real-data processing results demonstrates the validity of the proposed algorithm under the complex practical background. Compared with the CED algorithm, the proposed algorithm is more remarkable in real ionospheric decontamination.

6 Conclusions

This paper presents a novel ionospheric phase decontamination algorithm based on sparse reconstruction. The proposed algorithm transform the problem of estimating the modulation frequency of ionospheric phase contamination into a sparse optimization problem, and solve it by the simple iterative method rapidly to get the modulation frequency. In the proposed algorithm, the estimation accuracy of ionospheric modulation frequency is higher, thus the performance of phase decontamination is better and the the Bragg peak is sharper and target can be

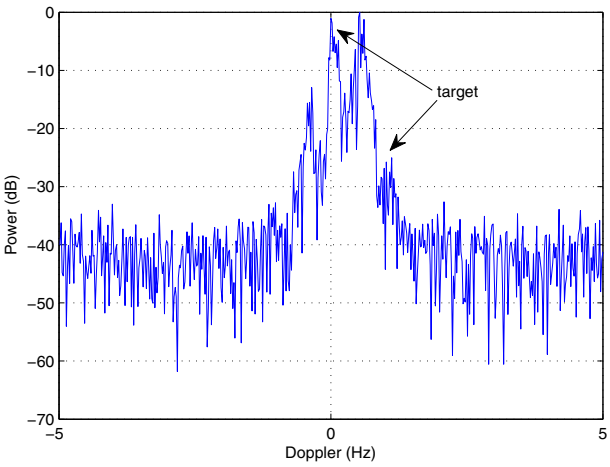

Fig. 12 The decontaminated real signal spectrum by the CED algorithm

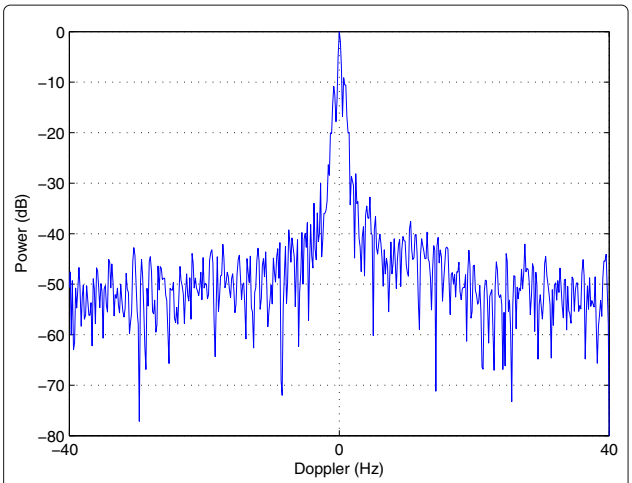

Fig. 14 The decontaminated real signal spectrum by the proposed algorithm

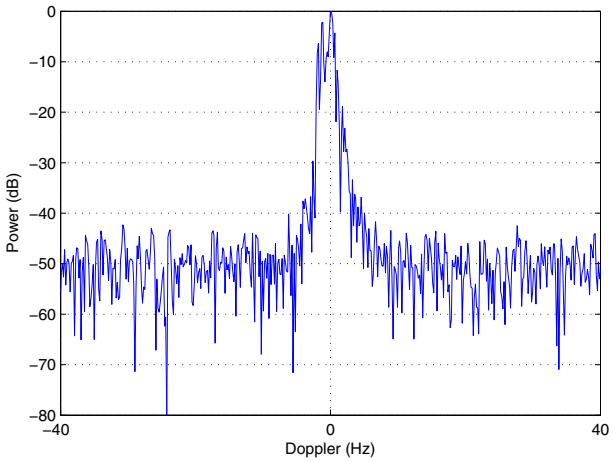

Fig. 15 The decontaminated real signal spectrum by the CED algorithm

discriminated in the Doppler spectrum. The simulation results show that, compared with CED algorithm, the decontamination performance of the proposed algorithm is better with the sharper Bragg peak which is beneficial for detecting the targets. Besides, the estimation precision of the proposed algorithm is higher under the situation of both slow and fast phase fluctuation or in the case of both high and low SNR. In real-data processing results, the proposed algorithm can clearly sharpen the peak spectrum and separate the low speed target spectrum from the sea clutter spectrum. Compared with the CED algorithm, the proposed algorithm is better.

Acknowledgements
This work was supported by the National Nature Science Foundation of China under Grant 61371184, 61301262, 61101173. The authors would like to thank the anonymous reviewers for insightful comments and helpful critiques of manuscript.

Competing interests
The authors declare that they have no competing interests.

Received: 15 December 2015 Accepted: 17 August 2016
Published online: 05 September 2016

References

1. JM Headrick, MI Skolnik, Over-the-horizon radar in the HF band. Proc. IEEE. **62**, 664–673 (1974)
2. AA Kolosov, *Over-the-Horizon Radar*. (Artech House, Boston, 1987)
3. Jf Chen, H Ma, CG Liang, YF Zhang, OTHR multipath tracking using the bernoulli filter. IEEE Trans. Aerospace Electron. Syst. **50**(3), 1974–1990 (2014)
4. K Lu, XZ Liu, Enhanced visibility of maneuvering targets for high-frequency over-the-horizon radar. IEEE Trans. Antennas Propagat. **53**(1), 404–411 (2005)
5. HT Su, HW Liu, PL Shui, Z Bao, Adaptive beamforming for nonstationary HF interference vancellation in skywave over-the-horizon radar. IEEE Trans. Aerospace Electron. Syst. **49**(1), 312–324 (2013)
6. G Fabrizio, F Colone, P Lombardo, A Farina, Adaptive beamforming for high-frequency over-the-horizon passive radar. IET Radar Sonar Navigat. **3**(4), 384–405 (2009)
7. J Duan, L Zhang, MD Xing, J Li, Transient interference excision and spectrum reconstruction with partial samples for over-the-horizon radar. IET Radar Sonar Navigat. **8**(5), 547–556 (2014)
8. YH Quan, MD Xing, L Zhang, Z Bao, Transient interference excision and spectrum reconstruction for OTHR. Electron. Lett. **48**(1), 42–44 (2012)
9. C Bo, H Gu, WM Su, J Chen, Ionosphere phase decontamination method based on subspace in sky-wave OTHR. Electron. Lett. **50**(24), 1874–1875 (2014)
10. A Bourdlillon, F Gauthier, J Parent, Use of maximum entropy spectral analysis to improve ship detection over-the-horizon radar. Radio Sci. **22**(2), 313–320 (1987)
11. J Parent, A Bourdlillon, A method to correct HF skywave backscattered signals for ionospheric frequency modulation. IEEE Trans. Antennas Propagat. **36**(1), 127–135 (1988)
12. PE Howland, DC Cooper, Use of the Wigner-Ville distribution to compensate for ionospheric layer movement in high-frequency sky-wave radar systems. IEE Proc. F: Radar Signal Process. **140**(1), 29–36 (1993)
13. K Lu, J Wang, XZ Liu, in *Proc. ICASSP 2003, 2nd edn*. A piecewise parametric method based on polynomial phase model to compensate ionospheric phase contamination (IEEE International Conference on Acoustics, Hong Kong, 2003), pp. 406–409
14. S Peleg, B Friedlander, The discrete polynomial-phase transform. IEEE Trans. Signal Process. **43**(8), 1901–1914 (1995)
15. K Lu, XZ Liu, YT Liu, Ionospheric decontamination and sea clutter suppression for HF skywave radars. IEEE J. Ocean Eng. **30**(2), 455–462 (2005)
16. MWY Poon, RH Khan, S Le-Ngoc, A singular value decomposition (SVD) based method for suppressing ocean clutter in high frequency radar. IEEE Trans. Signal Process. **41**(3), 1421–1425 (1993)
17. W You, ZS He, SL Wang, Ionospheric decontamination for skywave OTH radar based on complex energy detector. EURASIP J. Adv. Signal Process. **1**, 246 (2012)
18. P Maragos, JF Kaiser, TF Quatieri, On amplitude and frequency demodulation using energy operators. IEEE Trans. Signal Process. **41**(4), 1532–1550 (1993)
19. A Gholami, Sparse time-frequency fecomposition and some applications. IEEE Trans. Geosci. Remote Sens. **51**(6), 3598–3604 (2013)